Investigation of the earthquake ground motion coherence in heterogeneous non-linear soil deposits

F Gatti, Luciano de Carvalho Paludo, Angkeara Svay, Fernando Lopez-Caballero, Régis Cottereau, Didier Clouteau

Available online at www.sciencedirect.com

ScienceDirect

Procedia Engineering 199 (2017) 2354–2359

Procedia Engineering

www.elsevier.com/locate/procedia

X International Conference on Structural Dynamics, EURODYN 2017

Investigation of the earthquake ground motion coherence in heterogeneous non-linear soil deposits

F. Gatti[a,b,*], L. De Carvalho Paludo[a], A. Svay[a], F- Lopez-Caballero[a], R. Cottereau[a], D. Clouteau[a]

[a] *Laboratoire de Mécanique des Sols, Structures et Matériaux CNRS UMR 8579*
CentraleSupélec - Université Paris-Saclay
Grande Voie des Vignes Chatenay-Malabry, 92290, France
[b] *Dipartimento di Ingegneria Civile e Ambientale (DICA)*
Politecnico di Milano
P.zza Leonardo da Vinci 32, 20133, Milano, Italy

Abstract

The physics-based numerical simulation is a reliable tool to build-up source-to-site strong ground motion earthquake scenarios. In this paper, we enhance those forward simulations by including (1) the hysteretic non-linear behaviour of geomaterials and (2) the heterogeneous nature of soils. Scattering-induced damping, ground motion spatial incoherence and de-amplification may therefore be reproduced. A classical case study is considered herein: a seismic wave generated by a localized double-couple earthquake propagating towards the surface through layered elastic homogeneous bedrock, underlying a heterogeneous non-linear soil stratum. 3D numerical simulations were performed by means of a Spectral Element Method (SEM) code. The latter was coupled with a highly scalable random field generator to reproduce the media heterogeneity. Moreover, an extension to J_2 elasto-plasticity numerical integration was introduced. Time-histories and lagged-coherency curves at the surface show the ground motion de-amplification (mainly related to soil non-linearity) and loss of coherency (due to the wave-scattering caused by soil heterogeneity).

Peer-review under responsibility of the organizing committee of EURODYN 2017.

Keywords: Spectral Element Method, Non-linear, Heterogeneous, Wave-Propagation

1. Introduction

In recent years, classical seismological models have been successfully improved so as to explain the observed waveforms in sedimentary basins [1] or at the global scale [2]. To this end, the 3D source-to-site numerical simulation of strong ground motion earthquakes has become the leading and most reliable tool [3]. Large scale simulations comprehend the regional geology and topography. The incident wave-field is naturally radiated from a kinematic description of the fault mechanism. The Spectral Element Method (SEM) (i.e. high-order Finite-Element Method (FEM)) has recently become predominant due to its accuracy and straight-forward extension to parallel implemen-

* Filippo Gatti
E-mail address: filippo.gatti@centralesupelec.fr

1877-7058
Peer-review under responsibility of the organizing committee of EURODYN 2017.
10.1016/j.proeng.2017.09.232

tation [4]. Large scale 3D wave-propagation ($\approx 10^9$ dofs, with 10 points per minimum wavelength) in visco-elastic media has been successfully performed using the SEM, both at local and regional scales [5,6]. However, to model the spatial variability of seismic incident field (due to its significant effect on the structural response), the heterogeneous composition and the non-linear behaviour of soil deposits must be taken into account. In this paper, the SEM method was extended to model those two aspects consistently, to reproduce the ground motion incoherence. The test case considered is a seismic wave propagation problem within a 3-layer half-space (see Section 5). The uppermost soil layer is either modelled as elastic homogeneous, elastic heterogeneous, elasto-plastic homogeneous and elasto-plastic heterogeneous. The simulated wave-field at the surface is studied by comparing the synthetic time-histories, in terms of both ground motion coherency curve and soil layer spectral ratio. Section 2 discusses the efficient generation of 3D Gaussian scalar random-fields to represent the natural heterogeneity of the soil mechanical properties. A special attention is given to the overall numerical work-chain efficiency when tens of hundreds of processors are employed. Section 3 describes the hysteretic elasto-plastic model implemented. Section 4 addresses the strategy to coherently couple soil heterogeneity with the assumed non-linear mechanical behaviour. Finally, in Section 5, the results of the comparative study are presented.

2. Modelling soil heterogeneity by means of random field

A strategy to model heterogeneous media consists in considering the mechanical properties $\theta(\boldsymbol{x})$ as one stationary random field (featured at least by its average $\bar{\theta}(\boldsymbol{x})$ and its auto-covariance model $\mathcal{R}_\theta(\boldsymbol{x})$). The latter is then sampled at N_p integration points in the computational domain Ω: in the SEM, those are the Gauss-Lobatto-Legendre (GLL) integration points, at which both mass matrix and internal force vectors are computed. A realization of $\theta(\boldsymbol{x})$ is obtained by generating a Gaussian random field $G(\boldsymbol{x})$, whose Cumulated Distribution Function (CDF) is mapped point-wise (e.g., via the non-linear Rosenblatt transform [7]) to the desired first-order marginal density (e.g. log-normal).

Modelling soil heterogeneity in large scale domains implies a major computational effort: despite its characteristic dimension L ($\approx 10^4$ m) the computational grid must resolve both the wavelength and the heterogeneity correlation length $\ell_{c\theta}$ ($\approx 10^2$ m). To generate our random samples an open-source library ScaRL was used [8]. It uses the spectral representation technique [9]. In this method the random field $G(\boldsymbol{x})$ is generated as a sum of $N_\phi = N_x N_y N_z$ cosines with random phases, namely:

$$G(\boldsymbol{x}) = \sum_{n \leq N_\phi} \sqrt{2\mathcal{S}(\boldsymbol{k}_n)|\Delta \boldsymbol{k}|} \cos(\boldsymbol{k}_n \cdot \boldsymbol{x} + \phi_n) \tag{1}$$

Following this approach, the wave-number domain spanned by $\boldsymbol{k}$ is discretized over a regular grid of size $\boldsymbol{N} = \left[N_x, N_y, N_z\right]^T$, indexed by $\boldsymbol{n} = \left[n_x, n_y, n_z\right]^T$. $\mathcal{S}(\boldsymbol{k}_n)$ represents the power spectral density of the random field, whereas $|\Delta \boldsymbol{k}|$ is the unit volume in the spectral domain and the random variables ϕ_n are the independent elements of a $\boldsymbol{N}$-dimensional random variable with uniform density over $[0, 2\pi]$. The Fast Fourrier Transform can be used to bring the complexity of this generation method to $O(N_\phi \log N_\phi))$ [9] but it requires an uniform grid. Since the GLL points are not uniformly distributed in space, the random field must then be interpolated to the N_p GLL nodes.

When dealing with large domains ($L \gg \ell_{c\theta}$) ScaRL has a strategy to overcome the scalability issue. It generates realizations of $G(\boldsymbol{x})$ over the entire domain as superposition of I smaller independent realizations $G_i(\boldsymbol{x})$ supported on overlapping subdomains Ω_i of Ω [8]:

$$G(\boldsymbol{x}) = \sum_{i \in I} \sqrt{\psi_i(\boldsymbol{x})} G_i(\boldsymbol{x}). \tag{2}$$

where the set of functions $\psi_i(\boldsymbol{x})$ forms a partition of unity of Ω (that is to say $\sum_{i \in I} \psi_i(\boldsymbol{x}) = 1$ for any $\boldsymbol{x} \in \Omega$), supported by the set of subdomains Ω_i. Using this approach, the complexity becomes $O(n_p \log(n_p))$ where $n_p = N_\phi/\mathrm{P}$ and P is the number of processors. Essentially, this means that the scheme is $O(1)$ when we consider a constant number of GLL nodes per processor. The overlapping Eq. (2) involves an approximation that does not alter the average and variance of the resulting field $G(\boldsymbol{x})$ [8]. The influence on the correlation structure depends on the overlap, relative to the correlation length and has been studied in [8].

3. Modelling hysteretic soil non-linearity

The hysteretic material behaviour of the uppermost soil layer was modelled by exploiting a J_2-plasticity framework characterized by a von Mises failure criterion and a non-linear Frederick-Armstrong (FA) kinematic hardening rule (also called Chaboche's model)[10]. In this context, the yield locus is expressed in the deviatoric stress state as $f = \sqrt{\frac{3}{2}(\boldsymbol{s}-\boldsymbol{X}):(\boldsymbol{s}-\boldsymbol{X})} - \sigma_{yld}$ where $\boldsymbol{s}$ denotes the deviatoric stress tensor and $\boldsymbol{X}$ (called *back-stress tensor*) denotes the center of the yield surface ($f = 0$) in the deviatoric stress space (grey circle in Fig.1a). σ_{yld} represents the size the yield surface ($\frac{3}{2}$ times the yield-surface ratio). An isochoric non-associative flow rule is employed. The plastic

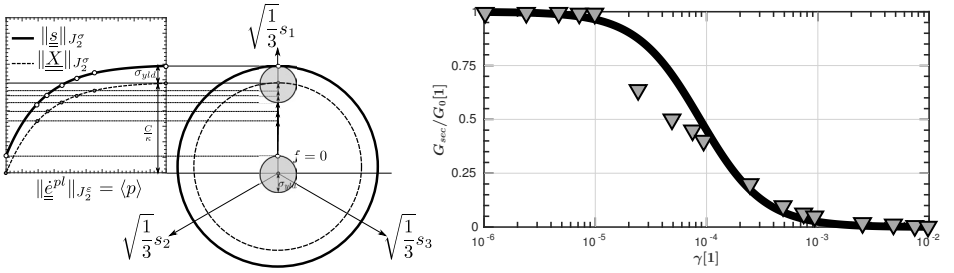

Fig. 1: (a) Norm of the deviatoric stress $\|\boldsymbol{s}\|_{J_2^\sigma}$ (black solid line) and back-stress $\|\boldsymbol{s}\|_{J_2^\sigma}$ (black dashed line) as a function of the plastic-strain norm $\|\dot{\boldsymbol{e}}^{pl}\|_{J_2^\varepsilon}$, according to the FA hardening rule. (b) Normalized decay curve obtained with the FA model, used to model the non-linear soil behaviour.

potential function g reads:

$$g = f + \frac{3}{4}\frac{\kappa}{C}\boldsymbol{X}:\boldsymbol{X} \tag{3}$$

with C and κ being the two parameters that rule the non-linear evolution of the kinematic hardening. Despite the non-associative flow rule ($f \neq g$), plastic flow is normal to the yield locus in the deviatoric plane. The plastic strain increment is non-negative and it undergoes the Kuhn-Tucker complementary conditions. The extra term $\frac{3}{4}\frac{\kappa}{C}(\boldsymbol{X}:\boldsymbol{X})$ represents the model's *fading memory*. The latter expression describes by the shift in the deviatoric plane of the yield locus's center $\boldsymbol{X}$: the critical state (i.e. hardening saturation) is achieved when the stress point lies both on $f = 0$ and on the yield limit surface (black solid line in Fig.1a). The described FA model is capable to reproduce the non-linear decay of the secant shear modulus G_{sec} with increasing shear distortion γ, as portrayed in Fig.1b. In this study, the mentioned decay curve is employed to define the non-linear soil behaviour, independently from its elastic properties (represented herein by the initial elastic shear modulus G_0).
The proposed non-linear model was introduced into the wave-propagation code SEM3D. The flow rule is numerically integrated via an explicit elasto-plastic predictor-multi-corrector algorithm.

4. Strategy to couple heterogeneous and non-linear soil behaviour

In this study, the initial shear modulus is represented by a random field $G_0(\boldsymbol{x}) = \rho V_S(\boldsymbol{x})^2$, where ρ is the homogeneous soil unit weight and $V_S(\boldsymbol{x})$ its shear wave velocity. Despite the local variation of the shear modulus, the set of parameters σ_{yld}-C-κ ruling the FA hardening rule (i.e. the back-stress evolution) were adjusted to follow the same normalized decay curve $G_{sec}(\boldsymbol{x})/G_0(\boldsymbol{x})$. The corresponding decay-curves of secant shear modulus G_{sec} are depicted in Fig.2b and they correspond to the normalized decay curve in Fig.1b. Fig.2a shows the stress-strain relationship ($\tau - \gamma$) issued from the FA model for randomly generated G_0 values. Hysteresis loops have the same shape but different amplitudes. From a practical point of view, a random field representing shear-wave velocities $V_S(\boldsymbol{x})$ (at GLL points) was generated at first, with the approach outlined in Sect.2. $V_S(\boldsymbol{x})$ was assumed to follow a log-normal distribution and the isotropic correlation length was set as ℓ_{C-Vs}=30m. $G_0(\boldsymbol{x})$ was computed accordingly and $C(\boldsymbol{x})$ was set to be equal to $G_0(\boldsymbol{x})$ to assure a smoother elastic-to-plastic transition (since C represent the value of the hardening module at first yield and zero plastic strain). As consequence, σ_{yld} and κ remain to be defined: the first is

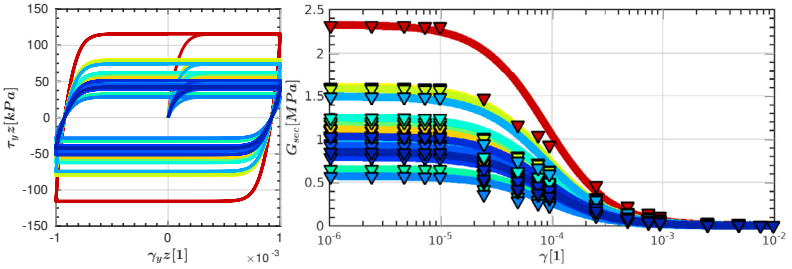

(a) (b)

Fig. 2: (a) Example of 20 cyclic shear stress-strain relationships ($\tau - \gamma$) for the Fredrick-Armstrong model, with randomly generated elastic shear modulus G_0. (b) 20 secant shear modulus decay curves according to the Fredrick-Armstrong model, corresponding to the $\tau - \gamma$ curves in (a). If normalized by the initial elastic shear modulus G_0, the decay curves in (b) correspond to the prototype curve in Fig.1b

fixed as $\sqrt{3}\rho V_S^2(\boldsymbol{x})\,\gamma_{el}$ (with γ_{el} being the shear-distortion at first yield, set equal to 10^{-5}). Considering an analogical 1D shear-test, the critical state is reached when the back-stress saturates (at large strains). The maximum shear stress τ_{max} is attained at this point and it is expressed as $\sqrt{3}\tau_{max} = \sigma_{yld} + C/\kappa$. From the latter expression, the local value of κ is straightforward determined, by either knowing τ_{max} values (for clays, it can be referred as as the Ultimate Strength Su) or estimating it upon correlation relationships with G_0 (see for instance [11]).

5. Case Study

A classical case study is considered herein: a seismic wave generated by a point-wise non-spherical source (i.e. a double-couple representing a pure-shear dislocation, indicated as SRC in Fig.3e) propagating towards the surface throughout a 3-layered domain is studied. The two deepest layers are considered homogeneous (HOM) linear-elastic (EL) materials. Due to the propagation in the layered substratum, the spherical wave-field radiated from SRC transforms into a planar incident wave impinging the lower soil layer interface. With this configuration, four simulations were performed and compared, by either considering the top-layer as (1) homogeneous linear-elastic (HOM-EL), (2) heterogeneous linear-elastic (HET-EL), (3) homogeneous non-linear (HOM-NL) and (4) heterogeneous non-linear (HET-NL) material. The domain is enveloped by Perfectly Matched Layers (PML), acting as absorbing boundary conditions. The effect of soil non-linearity and heterogeneity is at first described at three recording stations, namely: SRF1, SRF2 (at the surface) and INT (at the interface). Fig. 3a-3d show the velocigrams obtained at SRF1 and SRF2 (base-line corrected and high-pass filtered at 20 Hz): the two time-histories coincide in the homogeneous cases, as expected due to is plane and coherent wave-field. Typical *coda*-waves appear in the heterogeneous cases instead (Fig.3b-3d). Those late arrivals are symptomatic of an incoherent wave-field at SRF1 and SRF2. Clear de-amplification of the incident wave motion is presented for the two non-linear cases (Fig.3c-3d). The pseudo-acceleration response spectra Sa at point SRF1 (shown in Fig.3f) is highly influenced by the non-linear soil behaviour (depicted in terms of shear stress-strain relationship $\tau_{yz} - \gamma_{yz}$ in Fig.3g) at short period. Heterogeneity plays a minor role for the elastic case (≈25% of PGA reduction), whereas the short-period and peak Sa ordinates are remarkably de-amplified for HET-NL, with the respect to HOM-NL (≈21% of PGA reduction). This result is in accordance with the $\tau_{yz} - \gamma_{yz}$ curves in Fig.3g, where the HET-NL hysteresys loop is wider than HOM-NL, indicating the greater amount of energy dissipated. Another interesting aspect is the analysis of the ground motion coherency at the surface. The latter is a fundamental requirement for advanced seismic structural analysis. Coherency curves were computed for three different lag-distances (10, 20 and 30 m respectively), by applying a 11-point Hamming smoothing window [12]. For each lag-distance, the bin set were constructed by considering 40×40 points (i.e. 40 per direction). The mean of the log of the coherency curves was finally computed and shown in Fig.4. Fig.4a-4c show the lagged coherency for the four rheological models (HOM-EL, HET-EL, HOM-NL and HET-NL), at different lags. The homogeneous cases resulted to be coherent over a broad-band frequency range as expected, whereas the heterogeneous cases show the loss of coherency in the lower frequency band, decreasing after 10 Hz. The impact of the soil heterogeneity on the ground motion incoherence is clear even at small frequency and it appears more pronounced in the elastic case (Fig.4d) with

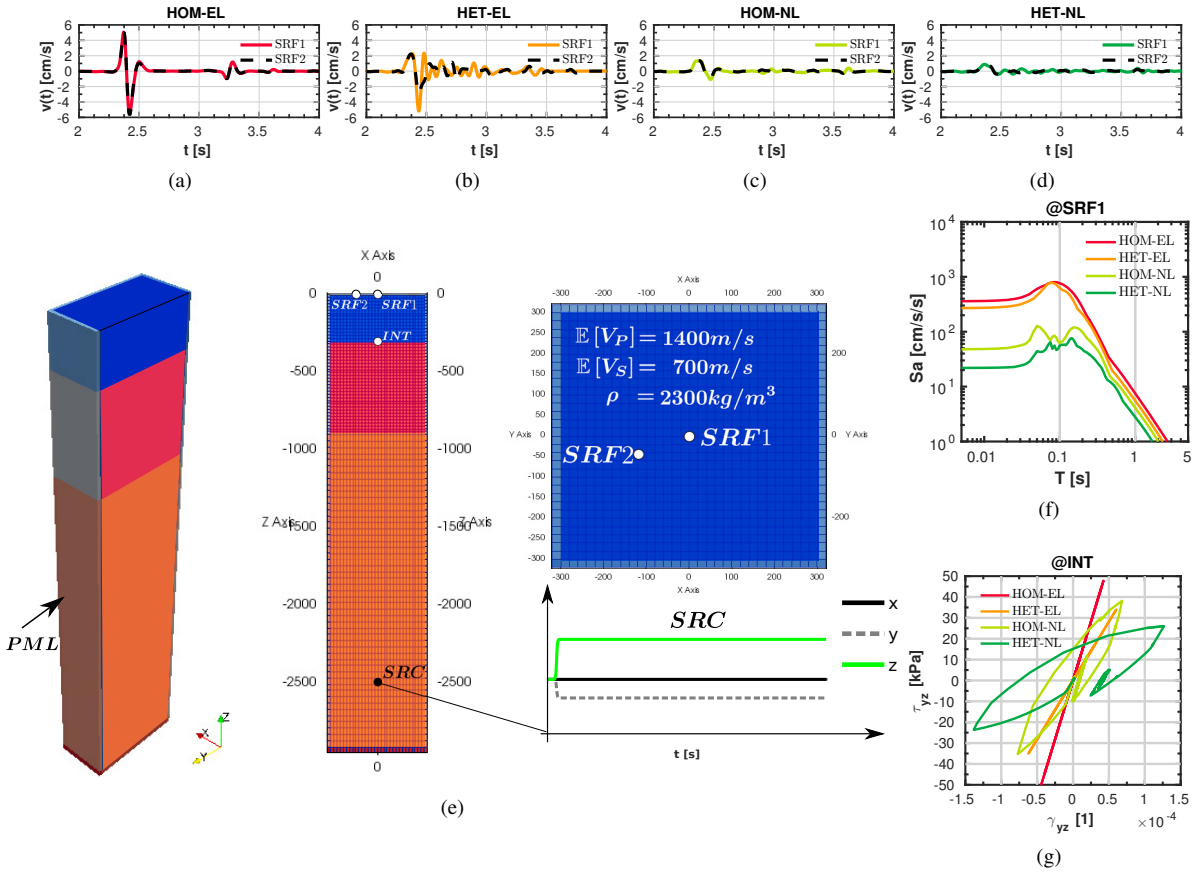

Fig. 3: (a-d) Synthetic velocigrams obtained at the surface for the four rheological models considered for the uppermost soil layer (HOM-EL, HET-EL, HOM-NL, HET-NL). (e) Clip and front/top views of the domain considered in the test case. The input displacement time-history at SRC is shown. SRF1, SRF2 and INT are employed as reference points. (f) Pseudo-Acceleration reponse spectra Sa at point SRF1. (g) Shear stress-strain relationship $\tau_{yz} - \gamma_{yz}$ at INT point.

respect to the non-linear one (Fig.4e). For HET-EL, the coherency loss is evident event at small lag-distance (i.e. coherency amplitude $|\gamma(\bar{f})| \approx 0.9$ for lag-distance of 10 m) and $|\gamma(\bar{f})|$ drops to values ≈ 0.6 for lag-distance of 30 m (comparable to ℓ_{C-V_S}). For a non-linear rheological model (HET-NL), $|\gamma(\bar{f})|$ stabilizes at above 0.75 between 0-10 Hz.

6. Conclusions

In this study, a parametric large scale numerical simulation of the seismic wave propagation in a non-linear-heterogeneous soil layer is presented, by exploiting the The Spectral Element Method. Numerical analyses are featured by the generation of soil heterogeneous mechanical properties by an efficient large random field generator. Moreover, a modified non-linear solver is employed to solve the dynamic equilibrium equation for elasto-plastic materials. The soil non-linearity mostly affects the ground motion de-amplification, whereas the soil heterogeneity produces incoherent ground motion at the surface. However, the non-linear decay of the shear modulus values seems to counteract the loss of coherency due to wave scattering. For the sake of brevity, a moderate source amplitude was considered herein. The effect of an increasing amplitude on the synthetics at the surface is interesting to be investigated (especially for a non-linear material behaviour). The preliminary parametric analysis presented herein may be extended also to the case of anisotropic correlation lengths of the shear-wave velocity (or other mechanical properties), which are estimated geological surveys and influence the recorded motion at the surface. In doing so, higher degrees of mesh refinement

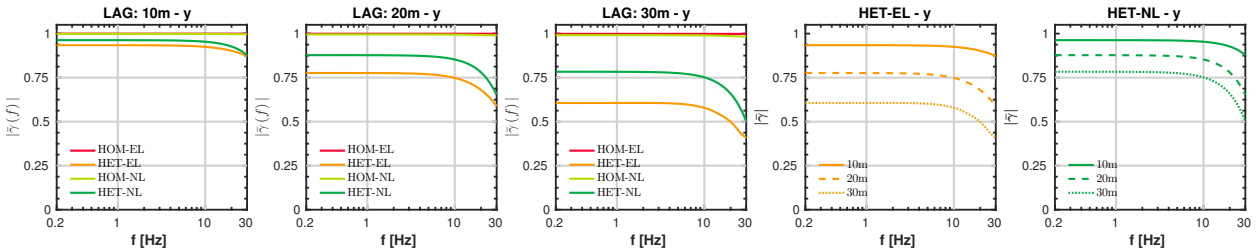

Fig. 4: Lagged coherency curves at the surface, for different lag-distances: (a) 10 m (SR) 20 m (c) 30 m. $|\bar{\gamma}(f)|$ represents the absolute value. In each plot, four coherency curves are depicted, one for each rheological models considered (HOM-EL, HET-EL, HOM-NL and HET-NL) for the uppermost soil layer. Lagged coherency curves for the HET-EL and HET-NL cases are depicted, one for each lag-distance considered (10 m, 20 m and 30 m), in (d) and (e) respectively.

should be considered so as to capture the extended frequency band of the surface signal, due to the wave-scattering effect.

Acknowledgements

This work, within the SINAPS@ project, benefited from French state funding managed by the National Research Agency under program RNSR Future Investments bearing reference No. ANR-11-RSNR-0022-04.

References

[1] R. W. Graves, D. J. Wald, Observed and Simulated Ground Motions in the San Bernardino Basin Region for the Hector Mine, California, Earthquake, Bulletin of the Seismological Society of America 94 (2004) 131–146.
[2] D. Komatitsch, J. Tromp, Spectral-element simulations of global seismic wave propagation-I. Validation, Geophysical Journal International 149 (2002) 390–412.
[3] R. Paolucci, I. Mazzieri, C. Smerzini, M. Stupazzini, Physics -Based Earthquake Ground Shaking Scenarios in Large Urban Areas, in: A. Ansal (Ed.), Perspectives on European Earthquake Engineering and Seismology, volume 1 of *Geotechnical, Geological and Earthquake Engineering - Vol.34*, Springer, 2014, pp. 331–359.
[4] D. Göddeke, D. Komatitsch, M. Möller, Finite and Spectral Element Methods on Unstructured Grids for Flow and Wave Propagation Methods, Springer, 2014, pp. 183–206.
[5] E. Faccioli, F. Maggio, R. Paolucci, A. Quarteroni, 2D and 3D elastic wave propagation by a pseudo-spectral domain decomposition method, Journal of Seismology 1 (1997) 237–251.
[6] D. Komatitsch, J.-P. Vilotte, The Spectral Element Method: An Efficient Tool to Simulate the Seismic Response of 2D and 3D Geological Structures, Bulletin of the Seismological Society of America 88 (1998) 368–392.
[7] M. Rosenblatt, Remarks on a multivariate transformation, The annals of mathematical statistics 23 (1952) 470–472.
[8] L. Paludo, V. Bouvier, R. Cottereau, D. Clouteau, Efficient Parallel Generation of Random Field of Mechanical Properties for Geophysical Application, in: 6th International Conference on Earthquake Geotechnical Engineering, 2015.
[9] M. Shinozuka, G. Deodatis, Simulation of stochastic processes by spectral representation, Applied Mechanics Reviews 44 (1991) 191–204.
[10] C. O. Frederick, P. J. Armstrong, A mathematical representation of the multiaxial Bauschinger effect, Materials at High Temperatures 24 (2007) 1–26.
[11] P. J. Vardanega, M. D. Bolton, Stiffness of Clays and Silts : Normalizing Shear Modulus and Shear Strain, Journal of Geotechnical and Geoenvironmental Engineering 139 (2013) 1575–1589.
[12] N. A. Abrahamson, J. F. Schneider, J. C. Stepp, Empirical Spatial Coherency Functions for Application to Soil-Structure Interaction Analyses, Earthquake Spectra 7 (1991) 1–27.